

Journal of Biomedical Optics

SPIEDigitalLibrary.org/jbo

***In vivo* imaging of hemodynamics and oxygen metabolism in acute focal cerebral ischemic rats with laser speckle imaging and functional photoacoustic microscopy**

Zilin Deng
Zhen Wang
Xiaoquan Yang
Qingming Luo
Hui Gong

In vivo imaging of hemodynamics and oxygen metabolism in acute focal cerebral ischemic rats with laser speckle imaging and functional photoacoustic microscopy

Zilin Deng,^{a,b*} Zhen Wang,^{a,b*} Xiaoquan Yang,^{a,b} Qingming Luo,^{a,b} and Hui Gong^{a,b}

^aWuhan National Laboratory for Optoelectronics-Huazhong University of Science and Technology, Britton Chance Center for Biomedical Photonics, 1037 Luoyu Road, Wuhan 430074, China

^bHuazhong University of Science and Technology, Key Laboratory of Biomedical Photonics of Ministry of Education, 1037 Luoyu Road, Wuhan 430074, China

Abstract. Stroke is a devastating disease. The changes in cerebral hemodynamics and oxygen metabolism associated with stroke play an important role in pathophysiology study. But the changes were difficult to describe with a single imaging modality. Here the changes in cerebral blood flow (CBF), cerebral blood volume (CBV), and oxygen saturation (SO₂) were yielded with laser speckle imaging (LSI) and photoacoustic microscopy (PAM) during and after 3-h acute focal ischemic rats. These hemodynamic measures were further synthesized to deduce the changes in oxygen extraction fraction (OEF). The results indicate that all the hemodynamics except CBV had rapid declines within 40-min occlusion of middle cerebral artery (MCAO). CBV in arteries and veins first increased to the maximum value of $112.42 \pm 36.69\%$ and $130.58 \pm 31.01\%$ by 15 min MCAO; then all the hemodynamics had a persistent reduction with small fluctuations during the ischemic. When ischemia lasted for 3 h, CBF in arteries, veins decreased to $17 \pm 14.65\%$, $24.52 \pm 20.66\%$, respectively, CBV dropped to $62 \pm 18.56\%$ and $59 \pm 18.48\%$. And the absolute SO₂ decreased by $40.52 \pm 22.42\%$ and $54.24 \pm 11.77\%$. After 180-min MCAO, the changes in hemodynamics and oxygen metabolism were also quantified. The study suggested that combining LSI and PAM provides an attractive approach for stroke detection in small animal studies. © 2012 Society of Photo-Optical Instrumentation Engineers (SPIE). [DOI: 10.1117/1.JBO.17.8.081415]

Keywords: ischemia; photoacoustic microscopy; laser speckle imaging.

Paper 11700SS received Nov. 29, 2011; revised manuscript received Jun. 21, 2012; accepted for publication Jul. 3, 2012; published online Jul. 31, 2012.

1 Introduction

Stroke is the leading cause of adult disability and the third most common cause of death worldwide.¹⁻³ For a noncommunicable disease, it is already and will continue to be the most challenging disease of increasing socioeconomic importance in aging populations. Among all types of stroke, ischemic stroke attributable to large-artery ischemia (most often middle cerebral artery, MCA) is the most common type and constitutes more than 80% of all strokes.^{1,3,4} Since there are rich nutrients and oxygen existing in the blood, the changes in cerebral hemodynamics and oxygen metabolism responsible for the local neuronal activities in ischemia often manifest blood flow supply, tissue oxygen consumption, and tissue viability.⁵⁻⁸ Also, the hemodynamic changes are key elements of ischemic pathophysiology, which can be depicted with imaging.⁹

Current well-established imaging modalities that have been adopted to study focal cerebral ischemia include computed tomography (CT), magnetic resonance imaging (MRI) and positron emission tomography (PET).^{1,3,10-13} They are all able to image cerebral blood volume (CBV) and cerebral blood flow (CBF) at different time point after stroke. However, CT is unable to image the oxygen saturation (SO₂) in vessels even with

contrast agent. MRI is only sensitive to deoxyhemoglobin (HbR). PET lacks sufficient spatial resolution and requires the intravenous administration of exogenous radioactive isotopes, which are inconvenient for continuous study in stroke. Optical imaging with high spatiotemporal resolution offers unique advantages and broad prospects for evaluating stroke physiology in endogenous contrast.¹⁴⁻¹⁶ It has greatly facilitated the monitoring of changes in cerebral hemodynamics.⁵

Up to the present, numerous different embodiments of optical imaging have been used to investigate the changes in cerebral hemodynamics after ischemia. Near-infrared spectroscopy (NIRS) could be adopted to identify the intermittent and spontaneous peri-infarct depolarizations (PID) during focal cerebral ischemia in rats.¹⁷ Multispectral optical imaging (MSOI) was demonstrated to map the changes in relative oxyhemoglobin (HbO) and relative HbR in forepaw stimulation in rat focal cerebral ischemia.¹⁸ Based on diffuse optical tomography (DOT), CBF, CBV, SO₂, and oxygen extraction fraction (OEF) were captured after 1 h occlusion of middle cerebral artery (MCAO) and reperfusion in rats.⁸ To yield high-resolution spatiotemporal maps of CBF and oxygen metabolism in focal cerebral ischemia simultaneously, laser speckle imaging (LSI) and MSOI had been used in combination.¹⁹ Although the previous investigations clearly visualized the physiological changes following focal cerebral ischemia, significant challenges remained. Among these imaging techniques, NIRS and DOT both lack sufficient

*These authors contributed equally to this work.

Address all correspondence to: Hui Gong, Wuhan National Laboratory for Optoelectronics-Huazhong University of Science and Technology, Britton Chance Center for Biomedical Photonics, 1037 Luoyu Road, Wuhan 430074, China. Tel: +86 027-87792933; Fax: +86 027-87792934; E-mail: huigong@mail.hust.edu.cn

spatial resolution to be effective for microvascular imaging. MSOI is a two-dimensional (2-D) imaging modality to image the average changes in cerebral hemodynamics of the regional cortical tissue and vasculature. Moreover, the baseline of optical properties and hemoglobin concentration should be first assumed.¹⁹⁻²¹ In a stroke, nerve cell viability and function are generally relevant to the hemodynamic signatures and oxygen consumption.^{8,22,23} It is difficult to monitor the changes in the aforementioned parameters with a single imaging modality. Therefore there is an intense interest in developing a new approach to accurately assess hemodynamic and metabolic changes from different vessels of the brain with high spatio-temporal resolution and eventually obtain a more comprehensive understanding of stroke.

LSI is a full-field optical technique to image blood flow changes *in vivo*. Without scanning, 2-D distribution of CBF can be obtained with high spatial and temporal resolution.^{24,25} Up to now, LSI has been demonstrated to be highly effective at measurement of CBF in the studies of ischemia,^{26,27} cortical spreading depression (CSD) and other experimental paradigms.²⁸⁻³⁰ Photoacoustic imaging, combining the high contrast of optics and low scattering of ultrasound, is a fast growing imaging modality, which is capable of multi-scale imaging.^{5,31-34} Based on photoacoustic imaging, three-dimensional (3-D) neurovasculature can be mapped in endogenous contrast with high spatial resolution. Recently, dark-field photoacoustic microscopy (PAM) as a promising tool was widely used to assess changes in blood-oxygenation dynamics within the mouse brain,^{35,36} hemoglobin SO₂ variations in single vessels,³⁷ brain hemodynamic changes during rat forepaw electrical stimulation and so on.³⁸⁻⁴⁰

To reveal the complicated changes in cerebral hemodynamics and oxygen metabolism in stroke, CBF, CBV, SO₂, and OEF in two groups of rats were first recorded during 3-h acute focal ischemia with LSI and PAM, respectively. Then CBF, CBV, SO₂ in single vessels and the index of oxygen metabolism were imaged before, and after 180-min MCAO in six rats with these two imaging techniques together. The statistical analysis was also performed, and then the results were compared with other investigation.

2 Materials and Methods

2.1 Experimental Setups

The detailed description of the LSI is provided elsewhere.^{24,41} As shown in Fig. 1(a), laser from laser diode with power of 30 mW, wavelength of 660 nm was used to illuminate the rat cortex at about 30-deg incidence. The speckle pattern generated by the scattered laser and modulated by motion of the red blood cells was acquired through a stereomicroscope (Z16 APO, Leica, Germany) attached to a charge-coupled device (CCD) camera (QE 270XS, PCO Pixelfly, Germany) with 20-ms exposure time and 2 × 2 binning. The aperture diaphragm and variable attenuator were well controlled to ensure the average speckle size to be about two pixels. To achieve high spatial resolution, the laser speckle temporal contrast analysis (LSTCA) was adopted to calculate the speckle contrast according to the following formula:²⁵

$$C_t(x, y) = \frac{\sqrt{\frac{1}{N-1} \sum_{n=1}^N (I_{x,y}(n) - \bar{I}_{x,y})^2}}{\bar{I}_{x,y}}, \quad (1)$$

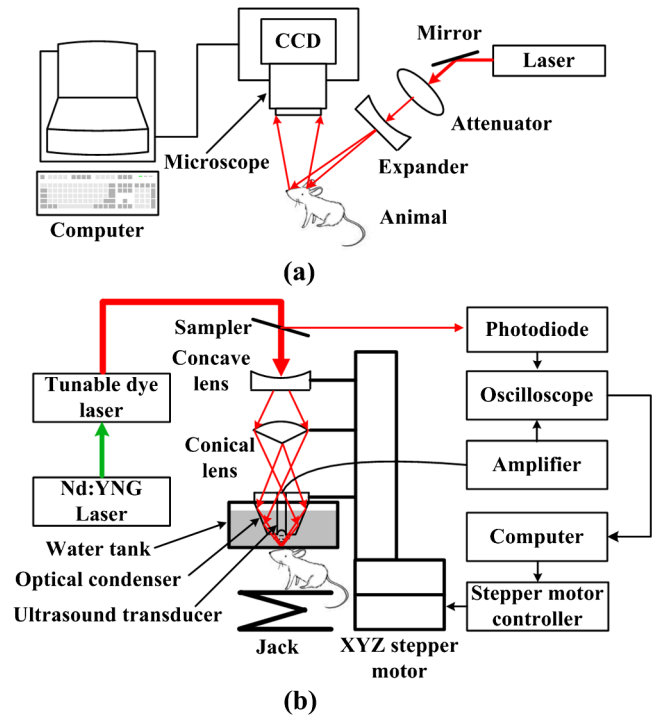


Fig. 1 Experimental setup of the imaging systems. (a) LSI; (b) PAM.

where $I_{x,y}(n)$ represents the intensity at pixel (x, y) in the n 'th raw speckle image. N describes the total number of frames and $\bar{I}_{x,y}$ indicates the average intensity at pixel (x, y) over the total N images. In our study, every frame of the speckle contrast image was acquired by analyzing the 100 consecutive raw speckle images with LSTCA based on GPU. So, it took 2 s to acquire the first CBF image and the time equivalent of the subsequent images is 20 ms. The speckle contrast image was then used to calculate the image of inverse correlation time values (ICT, arbitrary units) with a simplified approximation ($T/\tau_c \approx 1/C^2$, $T \gg \tau_c$), where T was the exposure time of the CCD and τ_c indicated the correlation time.²⁵ Here the ICT image was employed as the indicator of the CBF parameter and stored in a computer for further statistical analysis. Before the ischemic study, LSI was first used to image a group of sham MCAO rats with different geometrical position of optical elements and imaging target. This demonstrated that LSI can be adopted to compute the baseline of CBF.

PAM used for the rat brain imaging [Fig. 1(b)] was made in accordance with previous reports.^{42,43} A tunable dye laser (Cobra-stretch, Newport, USA) pumped by a Q-switched Nd:YAG laser (Surelite I-30, Continuum, USA) was adopted to induce photoacoustic signals. 6.5-ns laser light was firstly delivered through an optical fiber to the 3-D scanner. The energy of each laser pulse was detected by a photodiode connected with an oscilloscope for calibration. Then the beam was expanded and focused into the tissue with a ring-shaped area of illumination. The generated ultrasound was collected by a transducer with the focal region overlapping the optical focus. In the PAM used here, the ultrasonic detector has a center frequency of 50 MHz and a 70% nominal bandwidth. This enables the system to exhibit lateral and axial resolutions of 45 and 15 μm at the focus, respectively. At each location of the ultrasonic transducer, a depth-resolved photoacoustic wave can be recorded. If a 2-D raster scanning was implemented, the volumetric images of the

rat brain were acquired. Here, a step size of 30 μm was used. In our following experiments, the functional imaging was performed using three wavelengths: 576 nm, an HbO dominant wavelength, 584 nm, an isosbestic point of oxy- and deoxy-hemoglobin and 592 nm, a HbR dominant wavelength. Once the volumetric images were achieved, the maps of CBV can be acquired from the maximum amplitude projection (MAP) at 584 nm. Combining the resulting set of three-wavelength images, SO₂ in individual vessels could be calculated.³⁷ In the aforementioned three wavelengths, HbR and HbO are considered to be the dominant absorbing compounds in the blood. Thus the pressure rise P generated by the blood at each wavelength (λ_i) can be expressed as:

$$P(\lambda_i) = \Gamma\{\varepsilon_{\text{HbR}}(\lambda_i)[\text{HbR}] + \varepsilon_{\text{HbO}}(\lambda_i)[\text{HbO}]\}F(\lambda_i), \quad (2)$$

where Γ is the Grüneisen coefficient and F(λ_i) is the local light fluence (J/cm²). ε_{HbR}(λ_i) and ε_{HbO}(λ_i) represent the known molar extinction coefficients in cm⁻¹M⁻¹ of HbR and HbO, respectively. [HbR] and [HbO] describe the concentrations of the corresponding hemoglobin. With energy calibration and fluence compensation, the wavelength-independent optical fluence is achieved. The least-squares fitting gives the solution as:

$$\begin{bmatrix} [\text{HbR}] \\ [\text{HbO}] \end{bmatrix} = (M^T M)^{-1} M^T P K, \quad (3)$$

where

$$M = \begin{bmatrix} \varepsilon_{\text{HbR}}(\lambda_1) & \varepsilon_{\text{HbO}}(\lambda_1) \\ \varepsilon_{\text{HbR}}(\lambda_2) & \varepsilon_{\text{HbO}}(\lambda_2) \\ \varepsilon_{\text{HbR}}(\lambda_3) & \varepsilon_{\text{HbO}}(\lambda_3) \end{bmatrix},$$

$$P = \begin{bmatrix} P(\lambda_1) \\ P(\lambda_2) \\ P(\lambda_3) \end{bmatrix}$$

and K is a constant related to the system. Therefore, the SO₂ at each location can be calculated as:

$$\text{SO}_2 = \frac{[\text{HbO}]}{[\text{HbO}] + [\text{HbR}]}. \quad (4)$$

2.2 Animal Preparation

Specific pathogen-free rats were purchased from Wuhan University Center for Animal Experiment. Adult male Sprague-Dawley (SD) rats (280 to 350 g) used in the experiments were fasted except for water overnight. The rats were anesthetized with a mixture of 0.2 g/kg a-chloralose and 1 g/kg urethane administered intraperitoneally. Each anesthetized rat was placed on the stereotaxic head holder, and the scalp and muscle were pulled aside. A craniotomy of approximately 4 × 6 mm² size centered about 4.2-mm posterior and 3.1-mm lateral to Bregma, overlying the right parietal cortex was performed for each animal with a high-speed drill under constant saline cooling. The dura was kept intact. During the surgical operation, the body temperature of the rat was kept constant at 37 ± 0.5 °C with a heating pad. Then each rat was allowed to recover for at least 1 h. The physiological parameters were monitored and maintained within normal limits during the study. All animal experiments in the research were conducted by the Committee for the Care and

Use of Laboratory Animal at Huazhong University of Science and Technology.

2.3 Focal Cerebral Ischemia

The intraluminal suture occlusion of the middle cerebral artery was adopted to induce the acute focal ischemia.¹ After general surgical preparation and 1-h rest, the rat was turned to the supine position. The right common carotid artery (CCA) was carefully isolated from the soft tissues gently and ligated with a cotton thread. A poly-L-lysine-coated filament with diameter of 0.28 mm and a rounded tip of about 0.38 ± 0.02 mm was inserted through the external carotid artery into the internal carotid artery to occlude the MCA until the marker was completely inserted. In order to obtain the acute ischemic stroke, bilateral CCA was also ligated. Then the midline neck incision was sewed using surgical suture and some warm water was applied to the incision to prevent drying. Focal ischemia was confirmed for each rat with histologic analyses. Twelve hours after the occlusion, the animals were sacrificed and their brains removed from the cranium were stained with 2% 2,3,5-triphenyltetrazolium chloride (TTC) at 37°C for 30 min.⁸ At last, the dorsal sides of the stained sections were imaged with a camera.

2.4 Hemodynamic Parameters and Oxygen Metabolism Monitored During 3-H Acute Focal Ischemia in Rats

Twenty male SD rats were divided into two different experiments for dynamic functional changes. During 3-h acute focal ischemia, one group (n = 10) was used for CBF monitored with LSI and the other (n = 10) was used for CBV, SO₂, and OEF monitored with PAM. All the control hemodynamic parameters were acquired after 60 min surgical operation.

In the first experiment, LSI was adopted for mapping the 2-D distribution of CBF changes during ischemia as shown in Fig. 2(a). The baseline images were assessed 30 min before the acute focal ischemia. Immediately after the occlusion, the animal was placed on the animal holder and transferred to the system for data acquisition. However, it took about 15 min before the data collection started. So post-injury imaging was started approximately 15 min after MCAO. During 3-h ischemia, the changes in CBF were saved with time interval of 5 min. After 180 min of collecting ischemic distribution of CBF, each rat was allowed to recover on a heating pad.

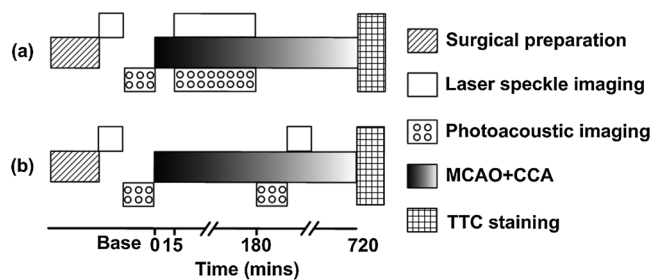


Fig. 2 The schematic designed for the monitoring of the changes in hemodynamics. (a) LSI and PAM used for the CBF and CBV, SO₂ and OEF monitoring within 180 min MCAO; (b) the study of the changes in hemodynamics and oxygen metabolism before and after 3-h MCAO with both LSI and PAM.

PAM was used to image the changes in CBV, SO_2 , and OEF in the other investigation. In this experiment, the control study was also carried out half an hour before ischemia. In order to confirm a successful occlusion, the distributions of CBF before occlusion and after 3-h ischemia were also imaged in the same rat, as shown in Fig. 2(a). To obtain the changes in CBV and SO_2 at the same time point with CBF monitored aforementioned, PAM was used for ischemic images 15 min after ischemia. Since the pulse repetition rate of the laser, which we used limits the current imaging speed in C-scan, a specific cross-section was chosen for dynamic functional images during ischemia with 5-min time interval. The selected cross-section was then repeatedly imaged at the aforementioned three wavelengths. After 180 min of occlusion, a 2-D scanning was also performed to indicate the monitored cross-section at 584 nm.

2.5 Changes in CBF, CBV, SO_2 and OEF After 3-H Acute Focal Ischemic Rats

Six male SD rats were used for the static study of changes in CBF, CBV, SO_2 , and OEF with both LSI and PAM after 3-h acute focal ischemia. After each rat recovered for 1 h from the surgical operation, the baseline CBF, CBV, and SO_2 were collected respectively as normal control. The schematic of study design is presented in Fig. 2(b). Thirty minutes after the control study, the acute focal ischemia in rats was induced. The changes of the ischemic CBF, CBV, and SO_2 were then acquired after 180 min of the occlusion.

2.6 Data Analysis

To investigate the relative changes in CBF at different vascular components, arteries and veins were identified by visual inspection through a microscopy and manually chosen corresponding to the regions in the images of CBF. Relative changes in CBF within the artery and vein were recorded over time as percent change of preischemic baseline. Thus each rat served as its own control. This process was done in each research here and the statistical analysis expressed as mean \pm standard error of mean (SEM) was then performed on a group dataset.

The same arteries and veins were investigated in photoacoustic imaging in the static study of changes in physiological parameters and oxygen metabolism after 3-h acute focal ischemia in rats. Compared with the images of CBF, the arteries and veins obtained by integrating over the full width at half-maximum of the vessels were identified in the MAP at 584 nm both before and after ischemia, respectively. The relative changes in CBV at each time were expressed as percent change from its baseline. Since it had been demonstrated the capability of PAM to image quantitatively static SO_2 in single vessels, the decrease of SO_2 both in artery and vein was expressed as absolute value from the control. The same process here was performed in all the experiments. The only difference which exists here is that in the dynamic functional images with PAM, the cross-section of artery and vein were mainly determined from the static SO_2 image before and after ischemia and the distribution of CBF was only used as a reference. The data from PAM was then used to calculate OEF:^{8,44}

$$OEF = (S_a O_2 - S_v O_2) / S_a O_2, \quad (5)$$

where $S_a O_2$, $S_v O_2$ were the SO_2 in artery and vein investigated.

3 Results

3.1 Hemodynamic Parameters and Oxygen Metabolism Monitored During 3-H Acute Focal Ischemia in Rats

A representative experiment for the continuous imaging and densely sampled longitudinal study in CBF during 3-h ischemia can be seen in Fig. 3. The qualitative maps of changes in CBF at isolated time points during occlusion are shown in Fig. 3(a).

Immediately after occlusion, there is an abrupt decrease in CBF in the region close to the anteriority and far from midline, which is approximately marked by the dotted line box in Fig. 3(a) –0 min. However, a slight increase exists in CBF in the region indicated by the dotted line circle and far from the anteriority and close to the midline [Fig. 3(a) –0 min to 40 min]. The MCAO produces the drop in CBF. However, the collateralization that occurs through the circle of Willis and leptomeningeal collaterals elevates the CBF in the region 2 [Fig. 3(a) –0 min].^{9,45,46} With increasing degrees of ischemia, CBF in the whole imaging window dropped and the ischemic infarct area was also increasing, especially in the region close to the anteriority and far from midline following a well-described progression in tissue infarction induced by MCAO.⁴⁷ These observations are consistent with some previous investigations.^{7,29,48}

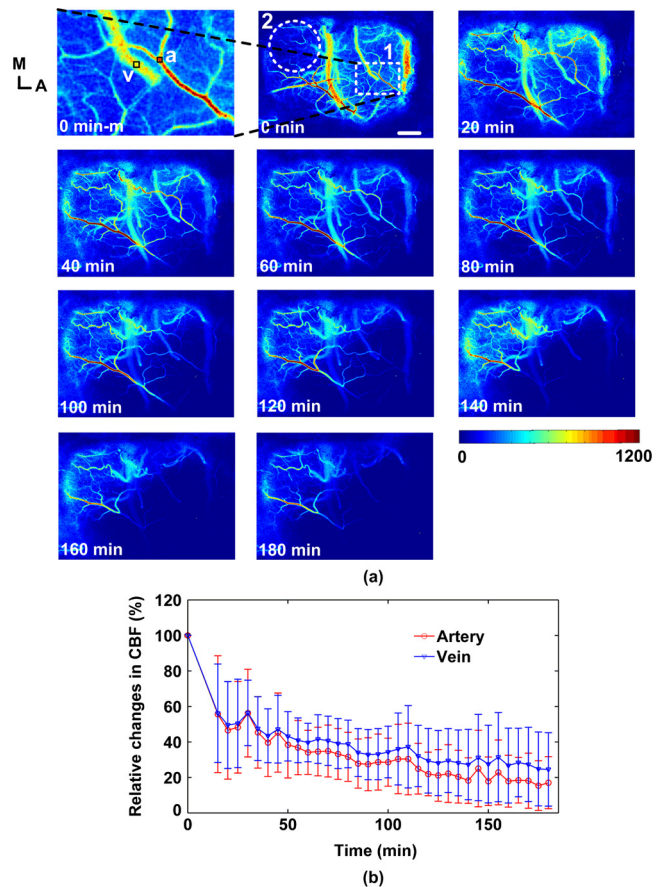


Fig. 3 CBF changes during 3-h ischemia. (a) The maps of the changes in CBF during 180 min MCAO of a typical experiment. The marked region by the dotted line box in Fig. 3(a) –0 min is depicted in Fig. 3(a) –0 min-m, where two vascular compartments indicated by solid squares and labeled with “a” and “v” were drawn for further statistical analysis. a, artery; v, vein; A, anterior; M, median. Scale bar: 1 mm. (b) The average time courses of the changes in CBF in arteries and veins.

The time courses of the relative changes in CBF for arteries and veins as depicted by “a” and “v” [Fig. 3(a)–0 min–m] can be found in Fig. 3(b), correspondingly. CBF exhibited a drastic reduction to $55 \pm 25.2\%$ of the control values both in arteries and veins just after 15-min occlusion and then it continued to decline slowly during the period of arterial occlusion. After 3-h MCAO, the CBF in arteries and veins dropped to $17 \pm 14.65\%$ and $24.52 \pm 20.66\%$ of its baseline, respectively.

Figure 4 displays a representative experiment for a rat monitored with PAM during 3-h acute focal ischemic stroke in MAPs. Compared with Fig. 4(a) and 4(b), the photoacoustic signal intensity decreased slightly in the whole imaging window. To perform the dynamic functional monitoring, a cross-section illustrated by the black dashed line in Fig. 4(b) was selected for repeatedly imaging.

Since 584 nm is an isosbestic absorption wavelength of hemoglobin, the photoacoustic signal is directly proportional to the total amount of hemoglobin (HbT) and the reduction of photoacoustic signal strength indicated that CBV changes in the vessels in the selected B-scan dropped in Fig. 4(c). At 592 nm, the molar extinction coefficient of HbR is greater than that of HbO. Based on the decrease in photoacoustic signals at 584 nm and increase at 592 nm, it is apparent that SO_2 in the vessels monitored declined as shown in Fig. 4(d). From Fig. 4(c) and 4(d), some structural changes existed in the first minutes in both images. After acute ischemia, the physiological state of the animals may fluctuate in a certain range to cause the recording unstabilized. In contrast with Fig. 4(c), there are several major

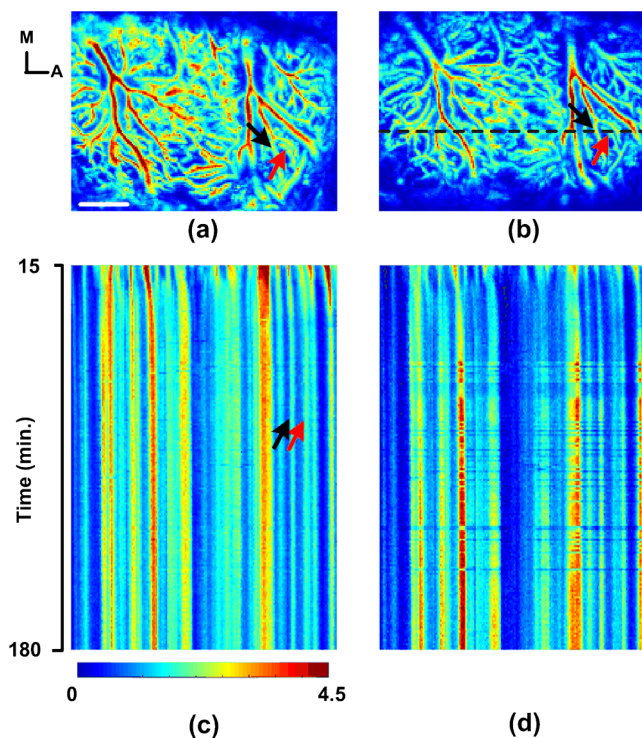


Fig. 4 Imaging results from the 3-h acute ischemic rats with PAM. (a) and (b) represent the distribution of CBV before and after ischemia at 584 nm. The vasculatures indicated by red and black arrows are artery and vein used to analysis, as well as in Fig. 4(c). A, anterior; M, median. Scalebar: 1 mm. The black dashed line in (b) illustrates the cross-section selected for repeatedly imaging in dynamic functional monitoring. (c) and (d) depict the projections of the chosen cross-section with B-scans acquired at 584 and 592 nm from 15 to 180 min post-ischemia.

fluctuations in photoacoustic signals in Fig. 4(d). These abrupt changes in photoacoustic signals are presumable to be induced by the spontaneous and repetitive PID. In the previous investigation, vasodilation induced by CSD caused the increase of arterial diameter.^{49,50} However, the small changes in diameter can be hardly distinguished by our current acoustic-resolution PAM. CSD also led the increase of SO_2 , which was produced by an increase in HbO concentration and a decrease in HbR concentration.⁴⁹ These results were consistent with ours.

The time traces of changes in CBV, SO_2 for two vascular components indicated by red and black arrows [Fig. 4(a), 4(b), and 4(c)] are plotted in Fig. 5. There is an overshoot by $12.42 \pm 36.69\%$ and $30.58 \pm 31.01\%$ in CBV for arteries and veins observed at 15 min following MCAO [Fig. 5(a)]. Thereafter, the CBV in the two selected vessels had a persistent reduction with small fluctuations and dropped to $62 \pm 18.56\%$ and $59 \pm 18.48\%$ of the control values after 180-min ischemia. This can be explained as follows. After ischemia, the vasodilation of resistance arterioles and veins which is known as autoregulation can increase the CBV to maintain the normal or slight decrease in CBF initially. However, when autoregulation is impaired, CBF and CBV will both decrease with further ischemia.^{51,52} Also, the hypercapnia is possible to cause the elevation of CBV just after the ischemia.⁸

The large changes in CBV during the first 40-min ischemia [Fig. 5(a)] lead to the relatively large reduction of SO_2 in arteries and veins existed in Fig. 5(b). It can also be referred to Fig. 3(b) where CBF has a relatively large decrease during the same time period. Then CBF and CBV both decline with a small slope and SO_2 reaches a relatively stable level with small fluctuations. For CBF and CBV both decline in ischemia, oxygen uptake rate should be improved to maintain the metabolism. After 3-h

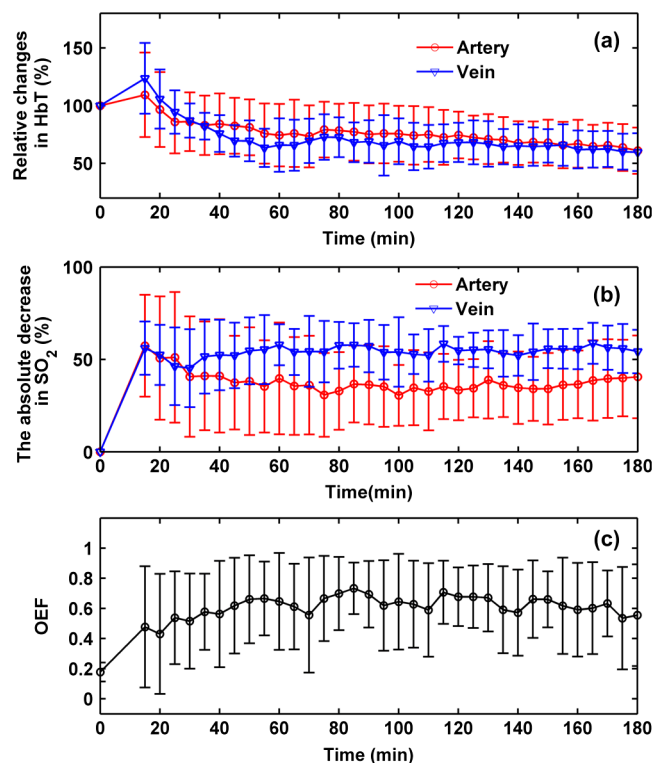


Fig. 5 The average time courses of the changes in HbT (a), SO_2 (b) at the two different vascular compartments and OEF (c) during 180-min MCAO.

occlusion, the reduction of SO_2 in arteries and veins reached $40.52 \pm 22.42\%$ and $54.24 \pm 11.77\%$ from their preischemic values and remained at this levels. Under these conditions, OEF increases from 0.18 ± 0.06 to 0.56 ± 0.34 [Fig. 5(c)].

3.2 Changes in CBF, CBV, SO_2 , and OEF after 3-H Acute Focal Ischemic Rats

Figure 6 illustrates the representative status of CBF and CBV before and after ischemia in the static study of changes in physiological parameters. From Fig. 6(a) and 6(b), it is apparent that as a result of 180-min MCAO, the CBF decreases seriously, especially in the regions close to the anteriority. This is because the MCAO used in these investigation produce early ischemic cell death in striatum to delayed infarction in the overlying frontal cortex following a well-described progression.⁴⁷ Compared with Fig. 6(c) and 6(d), CBV decreases significantly and a majority of microvessels disappear in the region far from the midline. This may be explained as follows. After the occlusion of the main artery, hypoperfusion of downstream microvasculature was induced. Although collateralization that occurs through the circle of Willis and leptomeningeal collaterals, there is still a serious shortage of hemoglobin.^{9,45} During the increase of ischemic time, brain microvascular beds are likely to be most vulnerable and haemorrhagic transformation (HT) will occur.^{53,54} With damage of brain microvessels, the blood-brain barrier will be caused disruption leading to the extravasation of blood.⁵⁵ All involved issues contribute to the CBV decreases so significantly that some vessels disappeared after 3-h ischemia.

The statistical changes in CBF, CBV, SO_2 in arteries and veins and OEF after 3-h acute focal ischemic stroke are indicated in Fig. 7. After the occlusion of 180 min, CBF in arteries and veins decrease to $17.73 \pm 12.38\%$ and $13.94 \pm 13.78\%$ owing to the hypoperfusion of downstream microvasculature

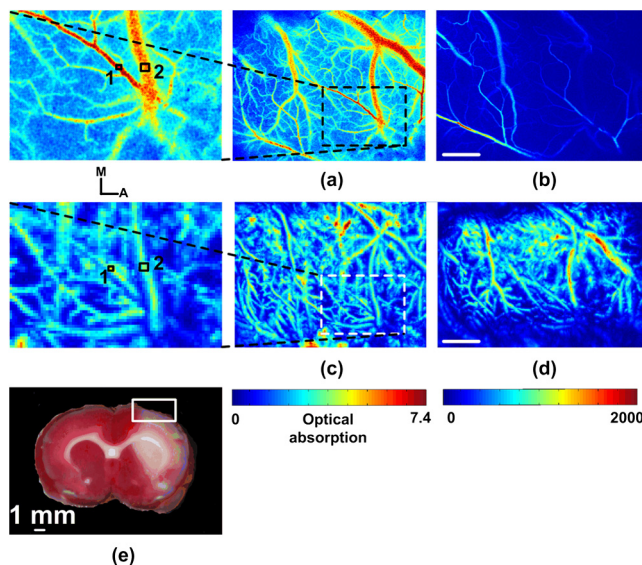


Fig. 6 Maps of changes in relative CBF and CBV after 3-h acute ischemic rats. (a) and (c) are the distribution of CBF and CBV before 3-h MCAO, where the vessels indicated by the solid line box marked with 1 and 2 show the artery and vein chosen for statistical analysis; (b) and (d) illustrate the distribution of CBF and CBV after 3-h MCAO; Scalebar: 1 mm. (e) Brain stained after MCAO procedure. The region marked by the solid box shows the approximate area of optical imaging. A, anterior; M, median.

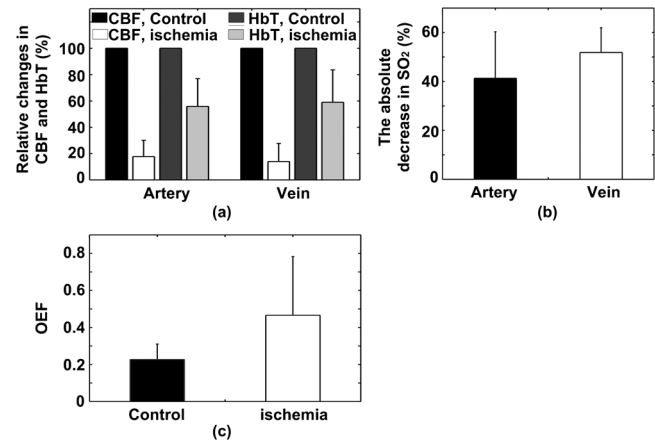


Fig. 7 Quantitative analysis of the relative changes in hemodynamics and oxygen metabolism after 180-min MCAO; (a) is the statistical relative changes in CBF and HbT at the two different vascular compartments; (b) the absolute decrease in SO_2 in artery and vein; (c) the changes in OEF.

and the corresponding CBV reduce to $55.83 \pm 21.05\%$, $58.98 \pm 24.58\%$, respectively [Fig. 7(a)]. The absolute SO_2 in arteries and veins decrease by $41.26 \pm 19.04\%$, $51.85 \pm 10.09\%$ compared with baseline conditions as seen in Fig. 7(b). The reduction in hemodynamic parameters is consistent with a stagnation and deoxygenation of blood in the vasculature after ischemia. For the decrease in CBF, CBV, and SO_2 , OEF increases from 0.18 ± 0.06 to 0.56 ± 0.31 in response to the changes. It is clear that CBF decreases most seriously after the occlusion. In the situation that CBF, CBV, and SO_2 decrease, oxygen uptake rate must be improved to maintain the cerebral oxygen metabolism.⁵² Compared with the preischemia, the conversion efficiency of HbO to HbR was increased after ischemia, which caused the more decrease in SO_2 in vein.

4 Discussion and Conclusion

In this pilot study, LSI and PAM were employed to yield the changes in CBF and PAM parameters including CBV, SO_2 , and OEF in response to acute ischemic injury in rat brains. With these techniques, the physiological parameters and oxygen metabolism parameters were able to separated and quantified. Compared with other investigation, a good agreement exists. Combining the investigation that CBV and OEF both increase to response the acute ischemia, two compensatory mechanism were established: autoregulation and increased OEF. The study suggests that combining LSI and PAM can provide an attractive approach for quantitative imaging of CBF and oxygen metabolism in the determination of the mechanism of stroke and detection.

Comparing with Fig. 4(c) and 4(d), several major fluctuations existed in photoacoustic signal at 592 nm, where there were nearly no changes at 584 nm. These discrepancies were maybe caused by PID in ischemia. At 584 nm, photoacoustic signals are only sensitive to CBV associated with the vessel diameter. Some previous researches suggested CSD induced the small increase of arterial diameter, where veins showed no obvious change in diameter.^{49,50} As our current acoustic-resolution PAM only had lateral resolution of $45 \mu\text{m}$ at focus, the small changes in diameter can be hardly discerned. So there were no obvious changes in Fig. 4(c), compared with some major fluctuations in photoacoustic signals in Fig. 4(d). CSD

was also accompanied by an increase in HbO concentration and a decrease in HbR concentration, which led the increase of SO_2 .⁴⁹ In Fig. 4(d), the decrease in photoacoustic signals in the several major fluctuations indicated the decrease in HbR concentration, for photoacoustic signal is more sensitive to the concentration of HbR at 592 nm. Certainly, the spontaneous and repetitive PID induced by ischemia were also reported by others.^{17,56}

By comparing the results of hemodynamics measured in static study and dynamic monitor with 180-min acute ischemic rats, only a small difference exists. We now discuss the results with the previous investigations.

4.1 CBF and CBV

Our results show that CBF in arteries, veins decreases to $34.13 \pm 12.39\%$, $39.65 \pm 10.83\%$ after 60 min ischemia and $17 \pm 14.65\%$, $24.52 \pm 20.66\%$ after 3-h MCAO. Correspondingly, CBV in arteries, veins reduces to $74.63 \pm 26.05\%$, $76.93 \pm 26.73\%$ after 1-h MCAO and $62 \pm 18.56\%$, $59 \pm 18.48\%$ of the control values after 180-min ischemia. Some groups have also reported the decrease in CBF and CBV. Jones et al. introduced that CBF dropped to less than 40% in the ischemic penumbra and 25% in the ischemic core after 1-h acute ischemia. Simultaneously, CBV decreased to less than 75% in the ischemic penumbra and 60% in the ischemic core.⁷ There have been DOT studies in rats that have shown CBF reduced to $\approx 42 \pm 4\%$ in response to 55 min MCAO.⁸ A study with MRI in gerbils has shown regions with CBF dropped to $52 \pm 17\%$, $36 \pm 18\%$ of the baseline have decrease in CBV to $91 \pm 17\%$, $72 \pm 21\%$ related to the control values.⁵⁷ Using LSI, Shin et al. observed that CBF dropped to less than 40% of the baseline after 60 min ischemia.⁴⁸ Also, Abookasis et al. used spatially modulated near-infrared illumination to demonstrate that there was a reduction about $23 \pm 5.4\%$ in CBV after 45-min acute ischemia.²⁰ There is a good similarity between our results and the investigation of other groups.

Based on our results, CBV in arteries and veins increases to the maximum value of $112.42 \pm 36.69\%$ and $130.58 \pm 31.01\%$ by 15-min MCAO. The increase in CBV in response to ischemia has been a consistent finding in other experimental studies of ischemia. Caramia et al. reported a CBV increase about 50% after 20-min MCAO.⁵¹ In the study on patients with subacute cerebral infarction, an increase in CBV was also demonstrated.⁵⁸ However, the CBF had a persistent reduction with small fluctuations during the entire ischemic period. The changes that CBV varied independently of CBF were also investigated by others. After ischemia, CBF will drop immediately. To maintain the CBF and metabolism, cerebral circulation will dilate to increase the CBV, a reflex known as autoregulatory.⁵² In the autoregulatory range, there is no or slight decrease in CBF. When its upper limit is exceeded, CBF will decrease rapidly.

4.2 SO_2

In the investigation, the absolute SO_2 in arteries and veins decreases by $41.26 \pm 19.04\%$, $51.85 \pm 10.09\%$ after 3 h ischemia. It is clear the reduction in SO_2 in vein is greater. This is because the OEF must increase to maintain tissue function and oxygen metabolism when the autoregulatory capacity is exhausted during the ischemia.⁵² The conversion efficiency of HbO to HbR was increased after ischemia which caused more decrease in SO_2 in vein. There are some other reports about the

decrease in SO_2 after ischemia. In the study from Culver et al. an ischemic region with the average SO_2 decrease by $11 \pm 4\%$ was visualized.⁸ With spatially modulated near-infrared illumination, a $21 \pm 2.2\%$ decrease in cerebral tissue SO_2 was recorded following 45-min cerebral ischemia.²⁰ Optical-resolution PAM was already applied to study ischemic stroke in a mouse model.⁴⁴ During ischemia, the average SO_2 in artery and vein dropped by 10% and 34%, respectively. There are significant differences among these results. This may be due to the use of different optical imaging modalities. It is important to note that MSOI is only able to image the average changes in cerebral hemodynamics of the regional cortical tissue and vasculature, whereas PAM adopted in this investigation can map the 3-D neurovasculature with high spatial resolution.

4.3 OEF

For the decrease in CBF, CBV, and SO_2 , OEF increases from 0.18 ± 0.06 to 0.56 ± 0.34 . In PET studies in a cat MCAO preparation, there is an increase about 120% to 200% in OEF.⁵⁹ With DOT, a $139 \pm 6\%$ increase in OEF was observed after about 1-h MCAO.⁸ It should be noted that OEF calculated in this investigation was based on single pial artery and single pial vein of cerebral vasculature. This may cause some quantitative errors when compared with other studies. Furthermore, we did not monitor the some of the systemic physiology parameters, such as blood gases, blood pressure, and glucose concentration. The absence of these parameters may affect the baseline of CBF, SO_2 , and OEF. However, the trend of CBF, SO_2 , and OEF are still comparable with these previous studies.

Overall, the trends and observation at different time points in this investigation agree well with similar results using other imaging techniques. Some discrepancies exist, and they are conducted in different imaging embodiments, different animal models, and different ischemic duration. Also, different analysis regions and different physiological parameters during the imaging may affect the results.

4.4 Others

It should be noted that LSTCA rather than laser speckle spatial contrast analysis (LSSCA) was employed to image the CBF changes during ischemia with LSI. The traditional LSSCA, based on calculation in the spatial domain with a spatial window, has low spatial resolution and statistical accuracy, impeding the applications in individual small vessels. However, LSTCA can compute the speckle contrast images with the original high spatial resolution, which makes it appropriate in applications on mapping CBF changes in single vessels. With different laser speckle contrast analysis methods, there may be a discrepancy existed in the study.

In PAM, to obtain the cerebral blood vessels with high spatial resolution, the skull was removed and the commercial ultrasound coupling gel was applied to the tissue surface to reduce the attenuation of the ultrasound signal. However, the coupling gel may affect the physiological environment of the brain. Therefore, carefully selection of coupling gel must be made. And the effect of coupling gel is desired to be investigated. This issue can also be solved by introduction of noncontact detection of ultrasound, which does not need any coupling agent. Since the current imaging speed is 30 A-line/s and mainly limited by the pulse repetition rate of laser pulse, only vascular segments in a specific chosen cross-section were monitored for

dynamic functional imaging during periods of arterial occlusion. With the imaging speed accelerated, a satisfactory C-scan should be performed at each time point. Limitation also existed regarding the employed MCAO models. It takes about 15 min to make the model and adjust the imaging system to start data collection. In fact, the changes in hemodynamics and oxygen metabolism during the first few minutes are the key elements for ischemia early diagnosis and treatment. These will be solved in our next work.

Acknowledgments

This work was supported by Science Fund for Creative Research Group of China (Grant No. 61121004), National Natural Science Foundation of China (Grant No. 81171067, 61078072), and the Specific International Scientific Cooperation (Grant No. 2010DFR30820).

References

1. A. Durukan and T. Tatlisumak, "Acute ischemic stroke: overview of major experimental rodent models, pathophysiology, and therapy of focal cerebral ischemia," *Pharmacol. Biochem. Behav.* **87**(1), 179–197 (2007).
2. U. Dimagli, C. Iadecola, and M. A. Moskowitz, "Pathobiology of ischemic stroke: an integrated view," *Trends Neurosci.* **22**(9), 391–397 (1999).
3. R. R. Moustafa and J. C. Baron, "Pathophysiology of ischemic stroke: insights from imaging, and implications for therapy and drug discovery," *Br. J. Pharmacol.* **153**(S1), S44–S54 (2008).
4. K. W. Muir et al., "Imaging of acute stroke," *Lancet Neurol.* **5**(9), 755–768 (2006).
5. S. Hu and L. V. Wang, "Photoacoustic imaging and characterization of the microvasculature," *J. Biomed. Opt.* **15**(1), 011101 (2010).
6. J. K.-J. Li, *Dynamics of the Vascular System*, World Scientific, Singapore (2004).
7. A. K. Dunn et al., "Simultaneous imaging of total cerebral hemoglobin concentration, oxygenation, and blood flow during functional activation," *Opt. Lett.* **28**(1), 28–30 (2003).
8. J. P. Culver et al., "Diffuse optical tomography of cerebral blood flow, oxygenation, and metabolism in rat during focal ischemia," *J. Cereb. Blood. Flow. Metab.* **23**(8), 911–924 (2003).
9. D. S. Liebeskind, "Imaging the future of stroke: I. ischemia," *Ann. Neurol.* **66**(5), 574–590 (2009).
10. D. D. McLeod et al., "Establishing a rodent stroke perfusion computed tomography model," *Int. J. Stroke* **6**(4), 284–289 (2011).
11. Q. Shen et al., "Functional, perfusion and diffusion MRI of acute focal ischemic brain injury," *J. Cereb. Blood. Flow. Metab.* **25**(10), 1265–1279 (2005).
12. M. Ibaraki et al., "PET measurements of CBF, OEF, and CMRO₂ without arterial sampling in hyperacute ischemic stroke: method and error analysis," *Ann. Nucl. Med.* **18**(1), 35–44 (2004).
13. L. F. Yu et al., "Spectral Doppler optical coherence tomography imaging of localized ischemic stroke in a mouse model," *J. Biomed. Opt.* **15**(6), 066006 (2010).
14. C. M. Niell and S. J. Smith, "Live optical imaging of nervous system development," *Ann. Rev. Physiol.* **66**, 771–798 (2004).
15. N. Pouratian et al., "Shedding light on brain mapping: advances in human optical imaging," *Trends Neurosci.* **26**(5), 277–282 (2003).
16. V. Ntziachristos, "Going deeper than microscopy: the optical imaging frontier in biology," *Nat. Methods* **7**(8), 603–614 (2010).
17. T. Wolf et al., "Noninvasive near infrared spectroscopy monitoring of regional cerebral blood oxygenation changes during peri-infarct depolarizations in focal cerebral ischemia in the rat," *J. Cereb. Blood. Flow. Metab.* **17**(9), 950–954 (1997).
18. J. Luckl et al., "The biological effect of contralateral forepaw stimulation in rat focal cerebral ischemia: a multispectral optical imaging study," *Front. Neuroenergetics* **2**(19), 1–9 (2010).
19. P. B. Jones et al., "Simultaneous multispectral reflectance imaging and laser speckle flowmetry of cerebral blood flow and oxygen metabolism in focal cerebral ischemia," *J. Biomed. Opt.* **13**(4), 044007 (2008).
20. D. Abookasis et al., "Imaging cortical absorption, scattering, and hemodynamic response during ischemic stroke using spatially modulated near-infrared illumination," *J. Biomed. Opt.* **14**(2), 024033 (2009).
21. H. K. Shin et al., "Normobaric hyperoxia improves cerebral blood flow and oxygenation, and inhibits peri-infarct depolarizations in experimental focal ischemia," *Brain* **130**(6), 1631–1642 (2007).
22. S. Hu and L. V. Wang, "Neurovascular photoacoustic tomography," *Front. Neuroenergetics* **2**(10), 1–7 (2010).
23. P. G. Haydon and G. Carmignoto, "Astrocyte control of synaptic transmission and neurovascular coupling," *Physiol. Rev.* **86**(3), 1009–1031 (2006).
24. J. Qiu et al., "Spatiotemporal laser speckle contrast analysis for blood flow imaging with maximized speckle contrast," *J. Biomed. Opt.* **15**(1), 016003 (2010).
25. S. Liu, P. Li, and Q. Luo, "Fast blood flow visualization of high-resolution laser speckle imaging data using graphics processing unit," *Opt. Express* **16**(19), 14321–14329 (2008).
26. C. Ayata et al., "Laser speckle flowmetry for the study of cerebrovascular physiology in normal and ischemic mouse cortex," *J. Cereb. Blood. Flow. Metab.* **24**(7), 744–755 (2004).
27. Q. Guo, G. Wang, and S. Namura, "Fenofibrate improves cerebral blood flow after middle cerebral artery occlusion in mice," *J. Cereb. Blood. Flow. Metab.* **30**(1), 70–78 (2010).
28. H. Bolay et al., "Intrinsic brain activity triggers trigeminal meningeal afferents in a migraine model," *Nat. Med.* **8**(2), 136–142 (2002).
29. A. K. Dunn et al., "Dynamic imaging of cerebral blood flow using laser speckle," *J. Cereb. Blood. Flow. Metab.* **21**(3), 195–201 (2001).
30. B. Choi, N. M. Kang, and J. S. Nelson, "Laser speckle imaging for monitoring blood flow dynamics in the in vivo rodent dorsal skin fold model," *Microvasc. Res.* **68**(2), 143–146 (2004).
31. M. H. Xu and L. H. V. Wang, "Photoacoustic imaging in biomedicine," *Rev. Sci. Instrum.* **77**(4), 041101 (2006).
32. L. V. Wang, "Prospects of photoacoustic tomography," *Med. Phys.* **35**(12), 5758–5767 (2008).
33. L. V. Wang, "Multiscale photoacoustic microscopy and computed tomography," *Nat. Photonics* **3**, 503–509 (2009).
34. X. D. Wang et al., "Noninvasive laser-induced photoacoustic tomography for structural and functional in vivo imaging of the brain," *Nat. Biotechnol.* **21**(7), 803–806 (2003).
35. E. W. Stein, K. Maslov, and L. H. V. Wang, "Noninvasive, in vivo imaging of blood-oxygenation dynamics within the mouse brain using photoacoustic microscopy," *J. Biomed. Opt.* **14**(2), 020502 (2009).
36. K. Maslov, G. Stoica, and L. H. V. Wang, "In vivo dark-field reflection-mode photoacoustic microscopy," *Opt. Lett.* **30**(6), 625–627 (2005).
37. H. F. Zhang et al., "Imaging of hemoglobin oxygen saturation variations in single vessels in vivo using photoacoustic microscopy," *Appl. Phys. Lett.* **90**(5) 053901 (2007).
38. V. Tsytisarev et al., "Photoacoustic microscopy of microvascular responses to cortical electrical stimulation," *J. Biomed. Opt.* **16**(7), 076002 (2011).
39. J. J. Yao et al., "Label-free oxygen-metabolic photoacoustic microscopy in vivo," *J. Biomed. Opt.* **16**(7), 076003 (2011).
40. H. F. Zhang et al., "Functional photoacoustic microscopy for high-resolution and noninvasive in vivo imaging," *Nat. Biotechnol.* **24**(7), 848–851 (2006).
41. Z. Wang et al., "Acute hyperglycemia compromises cerebral blood flow following cortical spreading depression in rats monitored by laser speckle imaging," *J. Biomed. Opt.* **13**(6), 064023 (2008).
42. X. Q. Yang et al., "High-resolution photoacoustic microscope for rat brain imaging in vivo," *Chin. Opt. Lett.* **8**(6), 609–611 (2010).
43. Z. L. Deng et al., "Two-dimensional synthetic-aperture focusing technique in photoacoustic microscopy," *J. Appl. Phys.* **109**(10), 104701 (2011).
44. S. Hu et al., "Optical-resolution photoacoustic microscopy of ischemic stroke," *Proc. SPIE* **7899**, 789906 (2011).
45. R. Khatri et al., "Leptomeningeal collateral response and extent of ischemic penumbra in patients with acute middle cerebral artery occlusion," *Neurology* **72**(11), A156–A156 (2009).
46. B. K. Menon et al., "Does presence of vascular risk factors and elapsed time from stroke onset affect leptomeningeal collateral (LMC) recruitment in acute ischemic stroke?," *Stroke* **41**(7), E483–E483 (2010).
47. S. T. Carmichael, "Rodent models of focal stroke: size, mechanism, and purpose," *NeuroRx* **2**(3), 396–409 (2005).

48. H. K. Shin et al., "Vasoconstrictive neurovascular coupling during focal ischemic depolarizations," *J. Cereb. Blood. Flow. Metab.* **26**(8), 1018–1030 (2006).
49. X. L. Sun et al., "Simultaneous monitoring of intracellular pH changes and hemodynamic response during cortical spreading depression by fluorescence-corrected multimodal optical imaging," *Neuroimage* **57**(3), 873–884 (2011).
50. E. Farkas, F. Bari, and T. P. Obrenovitch, "Multi-modal imaging of anoxic depolarization and hemodynamic changes induced by cardiac arrest in the rat cerebral cortex," *Neuroimage* **51**(2), 734–742 (2010).
51. F. Caramia et al., "Mismatch between cerebral blood volume and flow index during transient focal ischemia studied with MRI and Gd-BOPTA," *Magn. Reson. Imaging.* **16**(2), 97–103 (1998).
52. C. P. Derdeyn et al., "Variability of cerebral blood volume and oxygen extraction: stages of cerebral haemodynamic impairment revisited," *Brain* **125**, 595–607 (2002).
53. B. R. Thanvi, S. Treadwell, and T. Robinson, "Haemorrhagic transformation in acute ischaemic stroke following thrombolysis therapy: classification, pathogenesis and risk factors," *Postgrad. Med. J.* **84**(993), 361–367 (2008).
54. G. F. Hamann, Y. Okada, and G. J. del Zoppo, "Hemorrhagic transformation and microvascular integrity during focal cerebral ischemia/reperfusion," *J. Cereb. Blood. Flow. Metab.* **16**(6), 1373–1378 (1996).
55. G. J. del Zoppo, R. Von Kummer, and G. F. Hamann, "Ischaemic damage of brain microvessels: inherent risks for thrombolytic treatment in stroke," *J. Neurol. Neurosurg. Psychiatry.* **65**(1), 1–9 (1998).
56. J. Luckl et al., "Characterization of periinfarct flow transients with laser speckle and Doppler after middle cerebral artery occlusion in the rat," *J. Neurosci. Res.* **87**(5), 1219–1229 (2009).
57. G. Zaharchuk et al., "Is all perfusion-weighted magnetic resonance imaging for stroke equal? The temporal evolution of multiple hemodynamic parameters after focal ischemia in rats correlated with evidence of infarction," *J. Cereb. Blood. Flow. Metab.* **20**(9), 1341–1351 (2000).
58. C. Tsuchida et al., "Evaluation of peri-infarcted hypoperfusion with T2*-weighted dynamic MRI," *Jmri-J. Magn. Reson. Im.* **7**(3), 518–522 (1997).
59. W. D. Heiss et al., "Repeat positron emission tomographic studies in transient middle cerebral artery occlusion in cats: residual perfusion and efficacy of postischemic reperfusion," *J. Cereb. Blood. Flow. Metab.* **17**(4), 388–400 (1997).